nature nanotechnology

SUPPLEMENTARY INFORMATION

https://doi.org/10.1038/s41565-018-0318-5

In the format provided by the authors and unedited.

A DNA nanomachine chemically resolves lysosomes in live cells

KaHo Leung[1,2,3], Kasturi Chakraborty[1,2,3], Anand Saminathan[1,2] and Yamuna Krishnan[1,2*]

[1]Department of Chemistry, The University of Chicago, Chicago, IL, USA. [2]Grossman Institute of Neuroscience, Quantitative Biology and Human Behavior, The University of Chicago, Chicago, IL, USA. [3]These authors contributed equally: KaHo Leung, Kasturi Chakraborty. *e-mail: yamuna@uchicago.edu

A DNA Nanomachine chemically resolves lysosomes in live cells

KaHo Leung[1], Kasturi Chakraborty[1], Anand Saminathan and Yamuna Krishnan*

[1]*These authors contributed equally to this work.*

Supplementary Table 1 Sequences used for *ChloropHore* and *ChloropHore*$_{LY}$ assemblies. Oligo **P**, Oligo **C1** and Oligo **C2** combine to form *ChloropHore*. The sequences in matching colors are complementary.

	Sequence	Description
P	5'-BAC-NH_2-Lys-ATC AAC ACT GCA-Lys-COOH	PNA strand: [Cl^-] sensing module
C2	5'-TAT TGT GTA TTG TGT ATT GTT TTA TAT A***T***A TAG GAT CTT GCT GTC TGG TGT GCA GTG TTG AT-3'	Internal modification Alexa 647 on T with italic and bold
C1	5'-CAC CAG ACA GCA AGA TCC TAT ATA TAT ACC CCA ATC CCC AAT CCC CAA TCC CC-3'	3' modification with Alexa 546
C1-Br	5'-CAC CAG ACA GCA AGA TCC TAT ATA TAT ACC CCA ATC CCC AAT CCC CAA TCC CC-3'	3' modification with Alexa 546 C are 5'- Bromocytosines
C2 unlabelled	5'-TAT TGT GTA TTG TGT ATT GTT TTA TAT A***T***A TAG GAT CTT GCT GTC TGG TGT GCA GTG TTG AT-3'	
C1 unlabelled	5'-CAC CAG ACA GCA AGA TCC TAT ATA TAT ACC CCA ATC CCC AAT CCC CAA TCC CC-3'	
I^{mLY}_{OG}	5'-ATCAACACTGCACACCAGACAGCAAGATCCTATATATA-3'	5' modification with Oregon Green 488

Supplementary Table 2 Information of cells used in this study.

Sample	Sample number	Gene	Gene Mutation	Age (at sampling)
Normal individual 2	GM08429	N/A	N/A	M (1 DA)
Normal individual 3	AG01518	N/A	N/A	M (3 DA)
NP-A patient 1	GM00112	SMPD1	L302P	M (10 Mo)
NP-A patient 2	GM13205	SMPD1	P330fsX382	F (2 Yr)
NP-A patient 3	GM16195	SMPD1	L302P	M (no data)
NP-B patient 1	GM03252	SMPD1	L302P	F (2 Fw)
NP-B patient 2	GM11097	SMPD1	negative for the three most common mutations in SMPD1 (R496L, L302P and P330fsX382)	M (1 Yr)
NP-C patient 1	GM18414	NPC1	T1036M	F (no data)
NP-C patient 2	GM23162	NPC1	D948N	F (1 Yr)
NP-C patient 3	GM17910	NPC2	C93F	M (no data)

DA = day, Mo = month, Yr = year, Fw = fetal week

Formation of *ChloropHore*

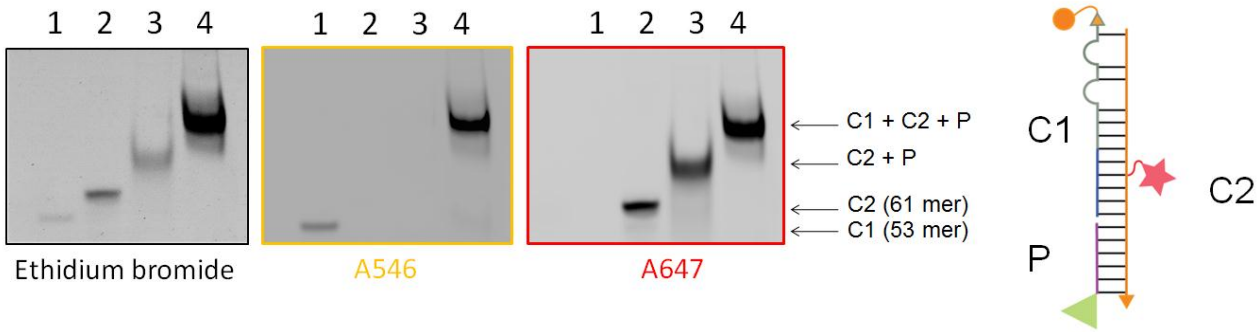

Supplementary Fig. 1 Formation of *ChloropHore*. Gel mobility shift assay showing the formation of *ChloropHore*. 12% Native PAGE run in 1× TBE buffer (pH 8.3) at 4°C. Lane 1: C1 2: C2, 3: C2+P 4: C1+C2+P (*ChloropHore*), in ethidium bromide, Alexa Fluor 546 and Alexa Fluor 647 channel. Experiments were performed in triplicate.

The formation of *ChloropHore* was validated by electrophoretic mobility shift assay utilizing native polyacrylamide gel electrophoresis (PAGE) (**Supplementary Fig. 1**). The hybridization of C2 and P1 was revealed by the lower mobility of sample (C2 + P) compare with sample C2 in ethidium bromide (EB) and Alex647 channel. Meanwhile, the lowest electrophoretic mobility of sample (C1 + C2 + P1) in EB, A546, A647 channel, indicates the formation of *ChloropHore* which constructed by C1, C2 and P1 in excellent yield.

Circular dichroism studies to validate conformational change of *ChloropHore*.

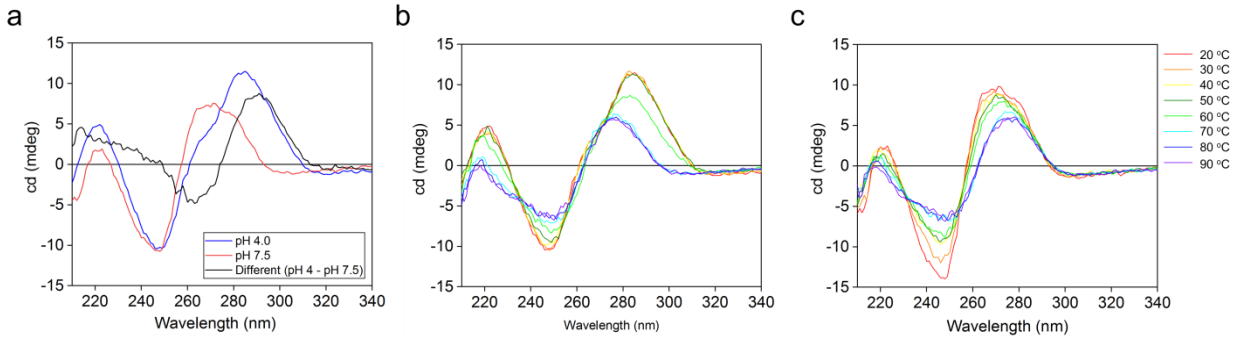

Supplementary Fig. 2 Characterization of *ChloropHore* by CD spectroscopy (a) CD spectra of *ChloropHore* at pH 7.5 (red), pH 4.0 (blue) and difference spectra (pH 4.0 – pH 7.5) is shown in black. Thermal denaturation was carried out on *ChloropHore* at **(b)** pH 4.0 as well as at **(c)** pH 7.5 to demonstrate i-motif formation. Experiments were performed in triplicate.

To validate the conformational change of *ChloropHore* upon acidification, circular dichroism (CD) spectrometer was employed to validate the structural change *in vitro*. *ChloropHore* shows a positive peak at 272 nm and a negative peak at 248 nm in pH 7.5 characteristic of duplex DNA. However, at pH 4.0, a positive peak at 285 nm and a negative peak at 248 nm was observed. The difference spectra of *ChloropHore* at pH 4.0 and pH 7.5 showed a positive peak at 292 nm and a negative peak at 263 nm which consistent with the CD signature of an i-motif. This was also how i-motif formation was proved in the parent *I-switch*[1,2].

Selectivity of *ChloropHore*

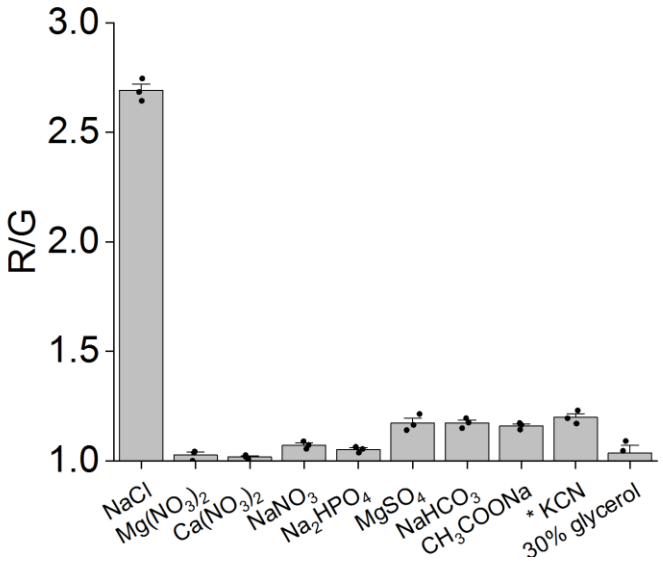

Supplementary Fig. 3 Response of *ChloropHore* (200 nM) given by the fold change in R/G from ~ 0 mM to 100 mM of all indicated ions and 30% glycerol. *2 mM. Error bars indicate the mean ± s.e.m. of three independent measurements.

In Figure 1, we already demonstrated the sensing characteristics of the H^+ sensing module is unaffected by integration to the Cl^- sensing module and vice versa thus enabling potential detection of these two ions in parallel. We investigated the response of *ChloropHore* to various ions such as $Mg(NO_3)_2$, $Ca(NO_3)_2$, $NaNO_3$, Na_2HPO_4, $MgSO_4$, $NaHCO_3$ and CH_3COONa and 30% glycerol (**Supplementary Fig. 3**). This reveals that the sensitivity of *ChloropHore* to diverse biologically abundant ions including Na^+, Ca^{2+}, Mg^{2+}, NO_3^- and PO_4^{3-} is negligible. BAC is also quenched by halides such as bromide and iodide (Br^- and I^-). However, the combined concentrations of all these ions including CN^- and SCN^- in biological cells are < 0.1% the value of chloride[3–5]. At this low

bioavailability, their contribution to the changes in BAC fluorescence in biological systems is negligible hence BAC acts as a chloride sensor in biological systems.

Design and characterization of *ChloropHore$_{Ly}$*

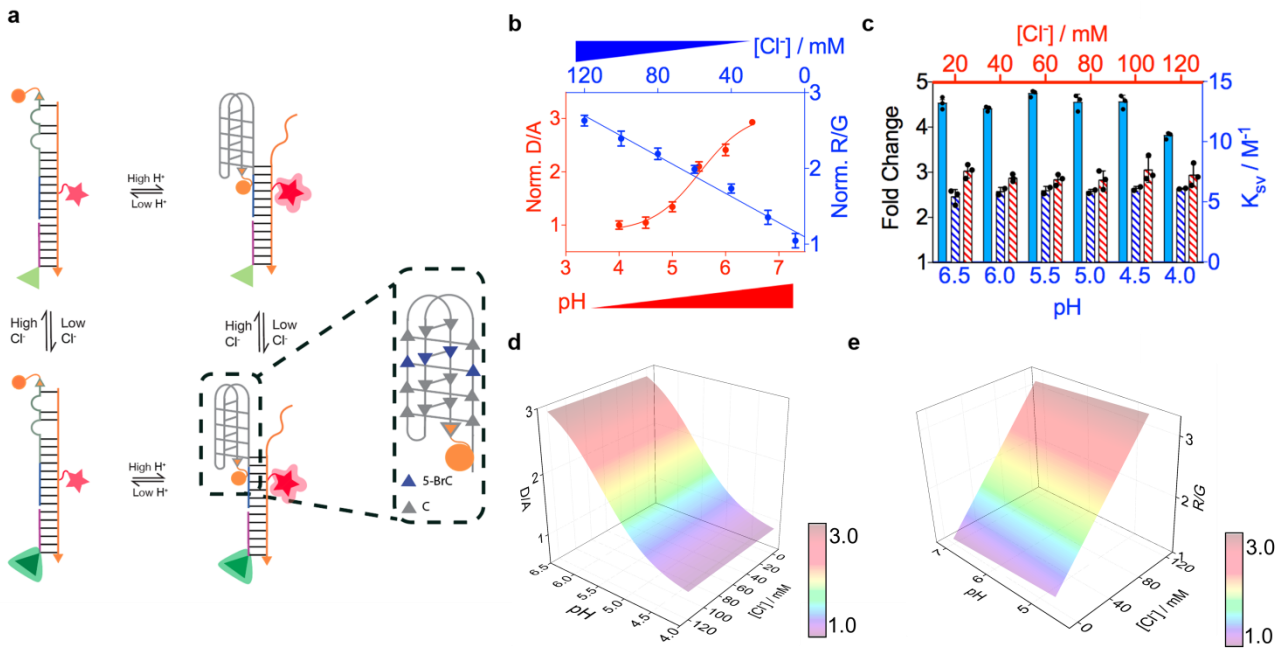

Supplementary Fig. 4 Design and characterization of *ChloropHore$_{Ly}$*. (**a**) Schematic of the working principle of *ChloropHore$_{Ly}$* in the "open state" (low FRET) at high pH and in the "closed" state (high FRET) at low pH while Cl^- sensitive fluorophore BAC displays high fluorescence in the absence of Cl^- ion whereas the fluorescence has been quenched by increasing concentration of Cl^- ions. Both pH and Cl^- sensing modules are independent of each other. *ChloropHore$_{Ly}$* incorporating brominated cytosines that has a more acidic pH sensing range (**b**) Normalized fluorescence intensity ratio (D/A) of donor (D, 570 nm when excited at 546 nm) and acceptor (A, 669 nm when excited at 546 nm) *in vitro* as a function of pH. *In vitro* Cl^- calibration profile of *ChloropHore$_{Ly}$* showing the normalized fluorescence intensity ratio (R/G) of Alexa 647 (R) and BAC (G) against increasing concentration of chloride ions. R/G values at different chloride concentrations were normalized to the value at 5 mM chloride. (**c**) The pH sensing module of *ChloropHore$_{Ly}$*, is insensitive to Cl^- concentration and Cl^- sensing module, is insensitive to pH. Performance of the pH and Cl^- sensing modules are in red and blue respectively. Plot of fold change of pH sensing modules in indicated Cl^- concentration (red dash). Fold change (blue dash) and K_{SV} (solid blue) for Cl^- sensing module versus pH. Fluorescence intensity ratio (**d)** D/A and (**e)** R/G of *ChloropHore$_{Ly}$* as a function of Cl^- and pH. Error bars indicate the mean ± s.e.m. of three independent measurements.

To enable sensing of pH < 5, we fine tuned the pH sensing regime of *ChloropHore*, using modified cytosines that was shown by us earlier to shift the pH sensing regime of the I-switch to more acidic regimes[6]. Consequently, *ChloropHore*$_{Ly}$ which introduces 5′-bromocytosines into the i-motif sequence, shows a pH sensing regime between pH 4.5−6.0 (**Supplementary Table 1** and **Supplementary Fig. 4a**). We investigated the fluorescence properties of *ChloropHore*$_{Ly}$ as a function of pH and [Cl^-], and determined its pH and Cl^- sensitivity. The D/A (Alexa546/Alexa647) ratio of *ChloropHore*$_{Ly}$ increases between 4.5 and 6.5 (**Supplementary Fig. 4b**) showing that it is well suited to measure the acidic pH of the mammalian lysosomes. *ChloropHore*$_{Ly}$ shows a sigmoid plot with no significant fold change in D/A over various concentrations of [Cl^-] (**Supplementary Fig. 4c,d**). Further, the R/G (Alexa647/BAC) ratio also shows a linear relationship with *ca.* 2.5 fold change upon increasing concentration of [Cl^-] from 5 mM to 120 mM. As expected, no significant variation of K_{sv} and fold change in R/G was observed when sweeping pH from pH 4.5–7.0 (**Supplementary Fig. 4c,e**). This indicates that the pH sensing and [Cl^-] sensing modules are independent of each other thus enabling the possibility of parallel detection of pH and [Cl^-] utilizing *ChloropHore*Ly.

Stability of *ChloropHore* in HDF cells

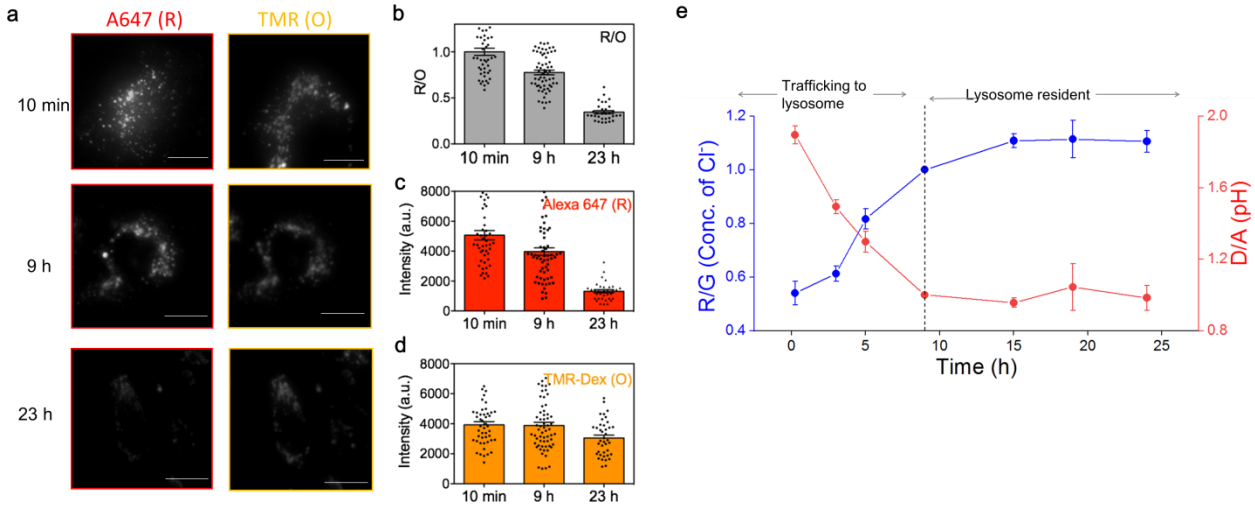

Supplementary Fig. 5 Stability of *ChloropHore* in HDF cells. (**a**) Representative images of HDF cells at indicated time points. Scale bar: 10 μm. Plots showing the (**b**) mean R/O ratio, (**c**) Alexa 647 labelled *ChloropHore* (R) channel and (**d**) TMR-Dex (O) channel whole cell intensity. Experiments were performed in triplicate. Error bars indicate the mean of cell intensity ± s.e.m. (n = 60 cells). Scale bar = 10 μm (**e**) Plot showing R/G ratios indicating increase of lumenal [Cl^-] (blue trace) and D/A ratios indicating increase of lumenal acidity (red trace) as a function of chase time. Error bars indicate the mean of three independent experiments ± s.e.m. (n = 25 cells, 250 endosomes)

As lysosomes are the degradation centers of the cell, we investigated the stability of *Chlorophore* in the lysosome. The fluorescence intensity ratio R/O at 9 h was ~25% less than that at the start, and after 23 h had only dropped to ~55%. This indicates ~75% of *ChloropHore* is intact within the lysosome. In patient samples, the degradation capacity is even lower, and an even higher amount of intact *ChloropHore* is expected. It is also well known that (a) all three dyes in *ChloropHore*$_{LY}$ leak out of the lysosome upon degradation of the DNA device (b) the timescales of degradation here are extremely slow compared to the timescales of sensor response and (c) thus any signal in the lysosome, is due to intact *ChloropHore*$_{\mathrm{Ly}}$. On the other hand, **Supplementary Fig. 5** reported the acidification and chloride ion accumulation upon endocytosis. It also demonstrated the ability of *ChloropHore*$_{Ly}$ to reported the pH change and chloride ion accumulation simultaneously in cell.

***in cellulo* performance of *ChloropHore*.**

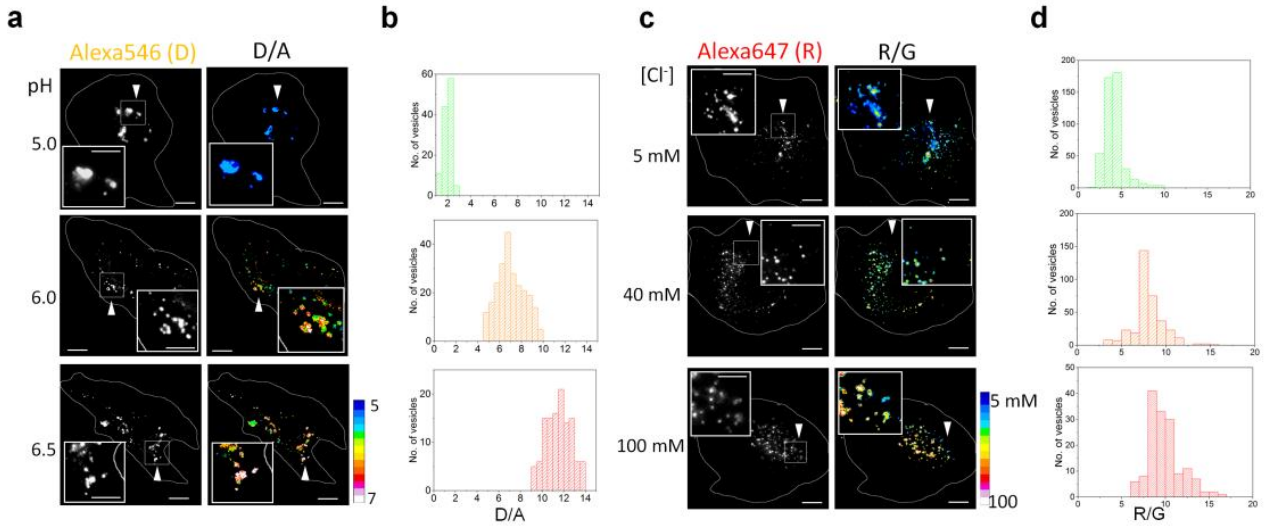

Supplementary Fig. 6 Intracellular calibration profile of *ChloropHore*. (**a**) Fluorescence images of primary human skin fibroblasts labeled with *ChloropHore* and clamped at the indicated pH and [Cl^-] = 100 mM, imaged in the donor channel and the corresponding pseudocolour pH map (**b**) Histograms of D/A ratios of endosomes at each pH (**c**) Fluorescence images of *ChloropHore* labeled fibroblasts clamped at the indicated [Cl^-], pH 5 shown in the Alexa 647 channel and respective pseudocolour [Cl^-] map. Scale bar = 10 mm and inset scale bar = 5 µm (**d**) Histograms of R/G ratios of endosomes at each [Cl^-]. Experiments were performed in triplicate (n = 15 cells, 150 endosomes).

To evaluate the intracellular pH and [Cl^-] sensing properties of *ChloropHore*, we clamped the cell with indicated pH and [Cl^-] buffers utilizing nigericin, monensin and tributyltin chloride (TBT-Cl) at high concentration of potassium ions. As shown in **Supplementary Fig. 6**, the plot of endosomal D/A ratio versus pH displays an increasing sigmoid curve from pH 5.0 to 6.5 with *ca.* 6.0–fold change in D/A. No significant difference was observed in when concentration of [Cl^-] was varied. In parallel, the plot of endosomal R/G ratio showed a linear dependence on [Cl^-], with *ca.* 2.5–fold change in R/G values from 5 mM to 100 mM [Cl^-] and no significant change of fold change in R/G or K_{sv} when pH was varied from pH 4.5–7.0. Both intracellular standard D/A ratio curve and R/G ratio line showed excellent correspondence with their *in vitro* profiles. Two 3D surface plots of R/G versus [Cl^-] at different pH values as well as D/A versus pH at different [Cl^-] values were generated (shown in the main figure). **Supplementary Fig. 7** shows the individual 2D *in cellulo* calibration profiles for each R/G against [Cl^-] and each D/A against pH. These results

indicate that post-endocytosis, the pH and [Cl^-] sensing properties of *ChloropHore in vitro* and *in cellulo* are highly consistent.

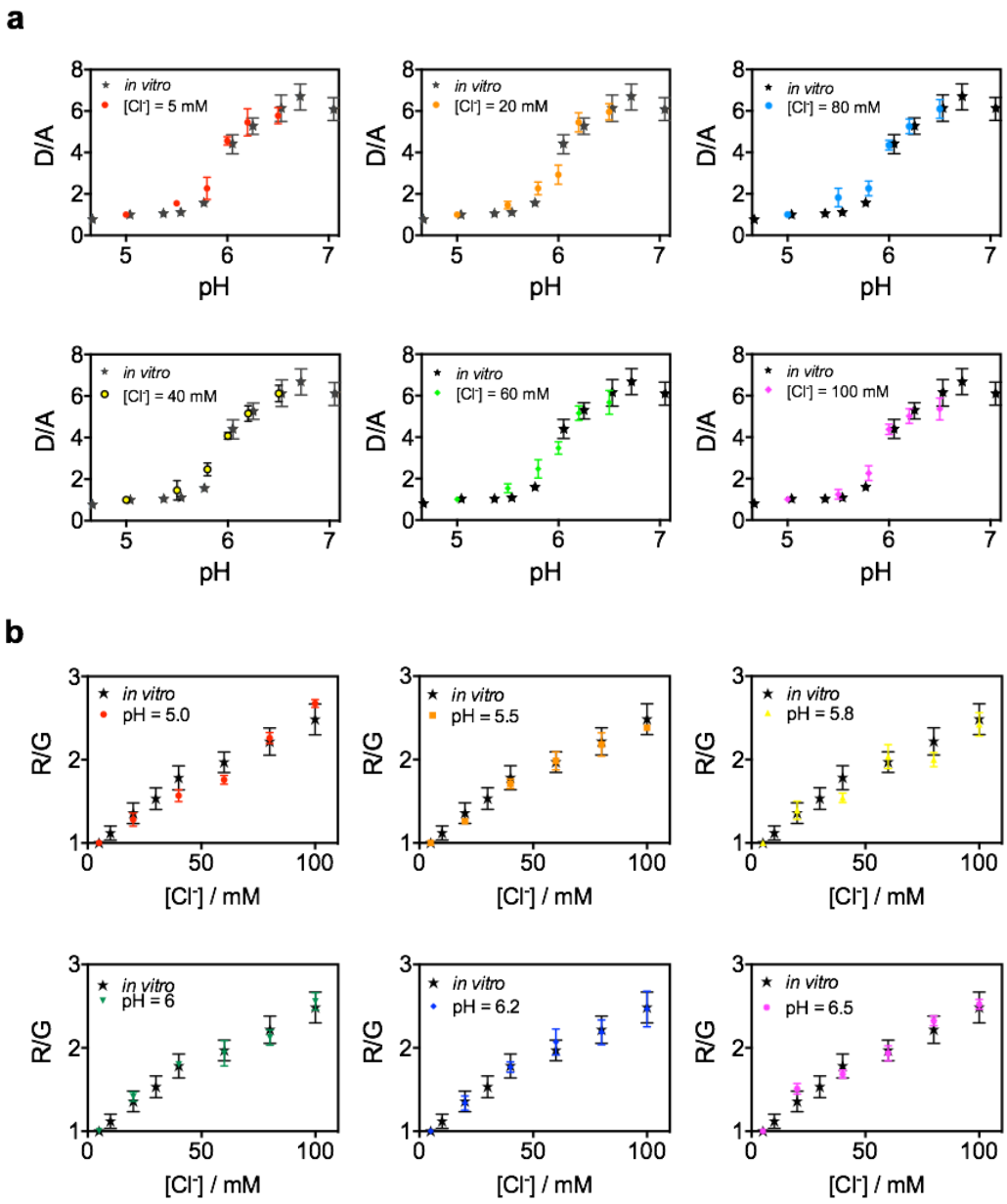

Supplementary Fig. 7 Intracellular calibration profile of *ChloropHore*. (**a**) D/A and (**b**) R/G ratio of *ChloropHore* as a function of pH and Cl^- inside the endosomes of human dermal fibroblasts each showing the intracellular calibration profile in the specified pH/Cl^- clamped condition (color dots). Error bars indicate the mean of three independent experiments ± s.e.m. (n = 15 cells, 150 endosomes)

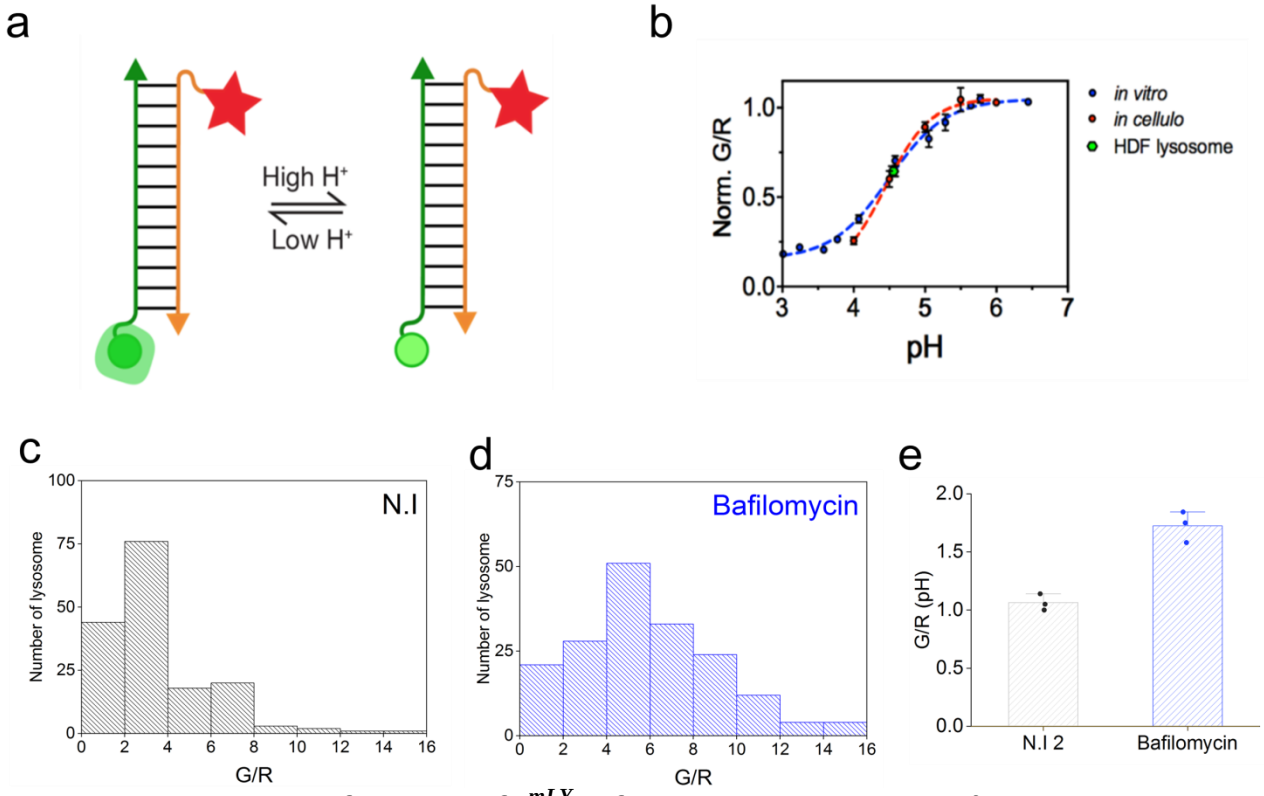

Supplementary Fig. 8. Performance of I^{mLY} in fibroblast. (**a**) Schematic of the working principle of I^{mLY} at low and high pH. pH indicator – Oregon green (OG) was conjugated into DNA and hybridize with its Alexa 647 labeled complementary. (**b**) *In vitro* (blue) and *in cellulo* (red) calibration curve of I^{mLY}. Histograms showing spread of G/R ratios of lysosomes of cells from a normal individual (c) without (gray) or (d) 500 nM bafilomycin A1(blue). (e) Bar graphs showing the mean lysosomal pH (G/R) ratios obtained from lysosomes of normal individual cells treated with or without 500 nM bafilomycin. Experiments were performed in triplicate. Error bars indicate the mean of three independent experiments ± s.e.m. (n = 15 cells, 150 lysosomes)

To find out the lysosomal pH of HDF cell, we employ I^{mLY} that pH sensing range is more suitable to detect the low lysosomal pH (< 5). We recently reported a ratiometric DNA-based sensor entitled I^{mLY} with pH detection range 4.0–5.5 which could perform the quantitative pH measurement in the lysosome of J774A.1 and THP-1 cells[7]. The fluorescence of OG (G) increases with the pH while the fluorescence of normalizing dye Alexa 647 (R) remains unchanged thus the fluorescence intensity ratio G/R (while G and R represent intensity of OG and Alexa 647 respectively) increase with increasing pH from 4 to 5.5 and a sigmoid profile has been observed (**Supplementary Fig. 8**).

We perform an *in cellulo* calibration of I^{mLY} in HDF cell to investigate the endosomal pH detecting ability of I^{mLY}. Encouragingly, the *in cellulo* calibration was well matched with the *in vitro* calibration profile, indicating that both sensor integrity and performance were quantitatively

preserved at the time of making lysosomal pH a measurements in these cells. Upon measurement using I^{mLY}, pH 4.6 was found for lysosome. This result demonstrates the capability of $ChloropHore_{LY}$ which revealing a pH detection range from 4.5 to 6.5, to measure the lysosomal pH and its variation.

To demonstrate that D/A and R/G specifically report lysosomal pH and [Cl^-] respectively, cells from normal individuals were treated with bafilomycin A1, a V-ATPase inhibitor or 5-nitro-2-(3-phenylpropylamino) benzoic acid (NPPB) a chloride channel blocker. V-ATPase inhibition depletes protons in the lysosome, and we expect major changes in D/A. NPPB is a chloride channel blocker, that, in lysosomes alters only chloride, but not pH. As expected, 2-IM profiles of bafilomycin A1 treated cells showed an overall increase of pH (G/R values) (**Supplementary Fig. 8c–e**).

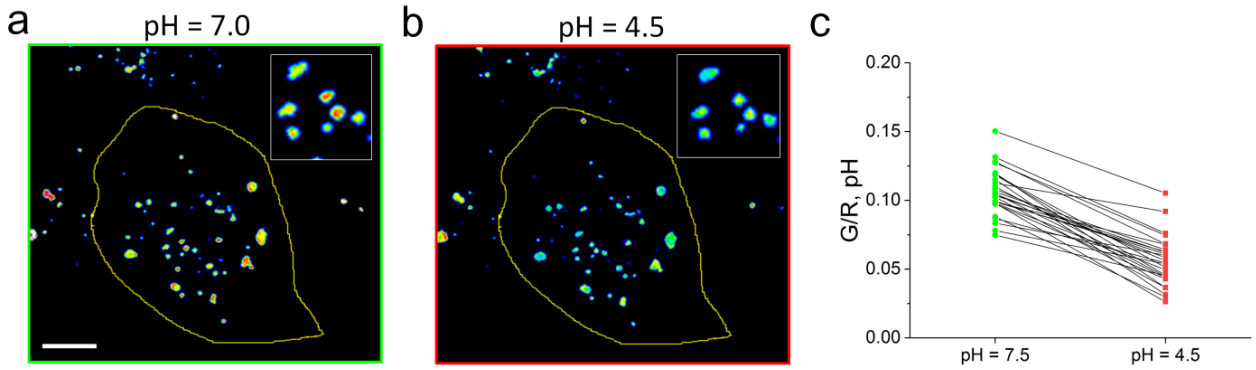

Supplementary Fig. 9 Quantitative performance of I^{mLY} within single lysosome. (**a**) Respective pseudocolour G/R map of normal individual skin fibroblast labeled with I^{mLY} and clamped at the indicated pH and [Cl^-] = 100 mM. Scale bars, 10 µm. (**b**) G/R change of lysosomes of cells that clamped with pH 7.5 and pH 4.5. Experiments were performed in triplicate (n = 15 lysosomes).

We have now performed the single lysosome clamping using *ChloropHore*$_{Ly}$ in parallel with reported ratiometric pH sensor I^{mLY}[7]. We clamped lumenal pH and [Cl^-] in HDF cells labeled with *ChloropHore* by incubation in clamping buffers of fixed pH and [Cl^-] containing nigericin, monensin and tributyltin chloride (TBT-Cl) at high [K^+][7,8]. Briefly, post-labeling with *ChloropHore*, HDF cells were fixed with 4% paraformaldehyde, incubated in the clamping buffer with desired ions for 1 h at 25℃. **Supplementary Fig. 9a–b** show representative fluorescence G/R images of cells clamped at the indicated pH and [Cl^-]. **Supplementary Fig. 9c** show single lysosome D/A and R/G values clamped at the indicated pH and [Cl^-] values. Upon clamping from pH 4.5 to pH 7.0 while [Cl^-] are remain constant at 100 mM, all of the lysosome displays an increased D/A while no significant variation of R/G was observed. On the other hand, the R/G of most lysosomes decrease significantly upon clamping from [Cl^-] = 100 mM to 5 mM while pH remain constant.

Labeling lysosome of BHK-21 cells

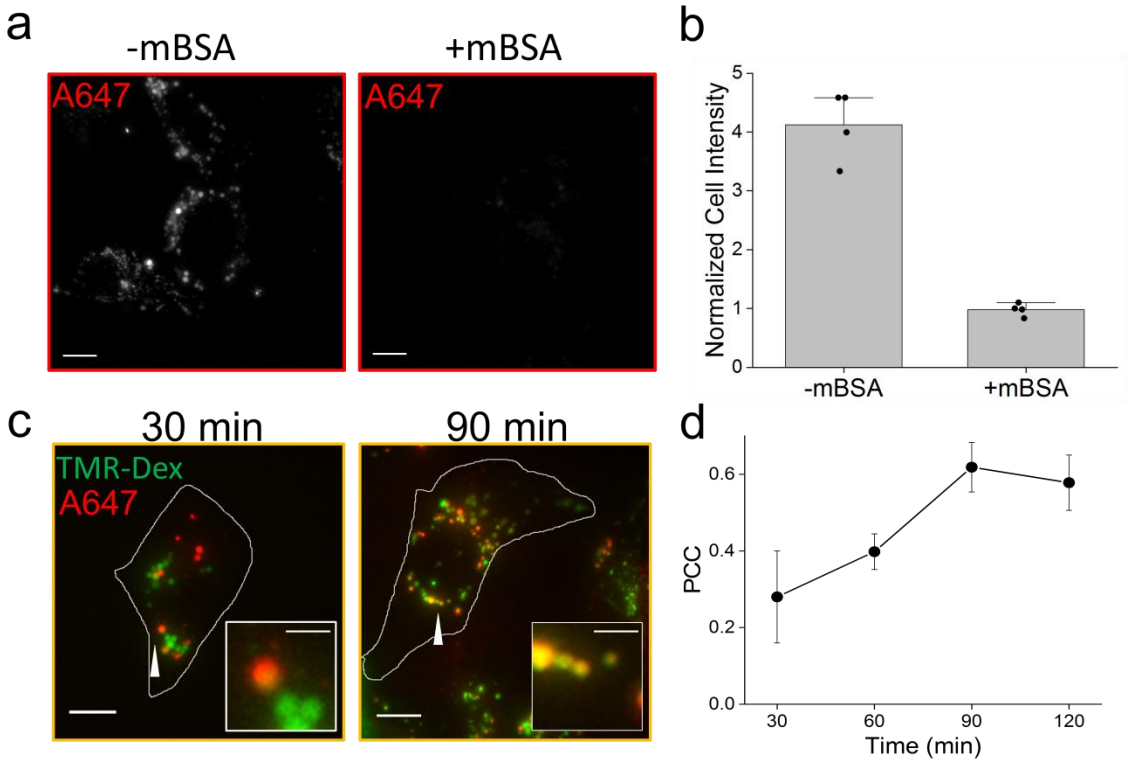

Supplementary Fig. 10 Labeling lysosome of BHK-21 cells (**a**–**b**) *ChloropHore* internalization by BHK-21 cells is competed out by excess maleylated BSA (mBSA, 10 μM), revealing uptake is by scavenger receptors. Cells are imaged in Alexa647 channel. (**c**) Representative images of lysosomes of HDF cells labelled with TMR dextran (TMR; G) by fluid phased endocytosis and by scavenger receptor mediated endocytosis of *ChloropHore* (Alexa647). (**d**) Pearson's correlation coefficient of colocalization between *ChloropHore* and lysosomes as a function of *ChloropHore* labeling chase times. Experiments were performed in triplicate. Error bars indicate the mean of four independent experiments ± s.e.m. (n = 20 cells).

Labeling lysosome of T47D cells

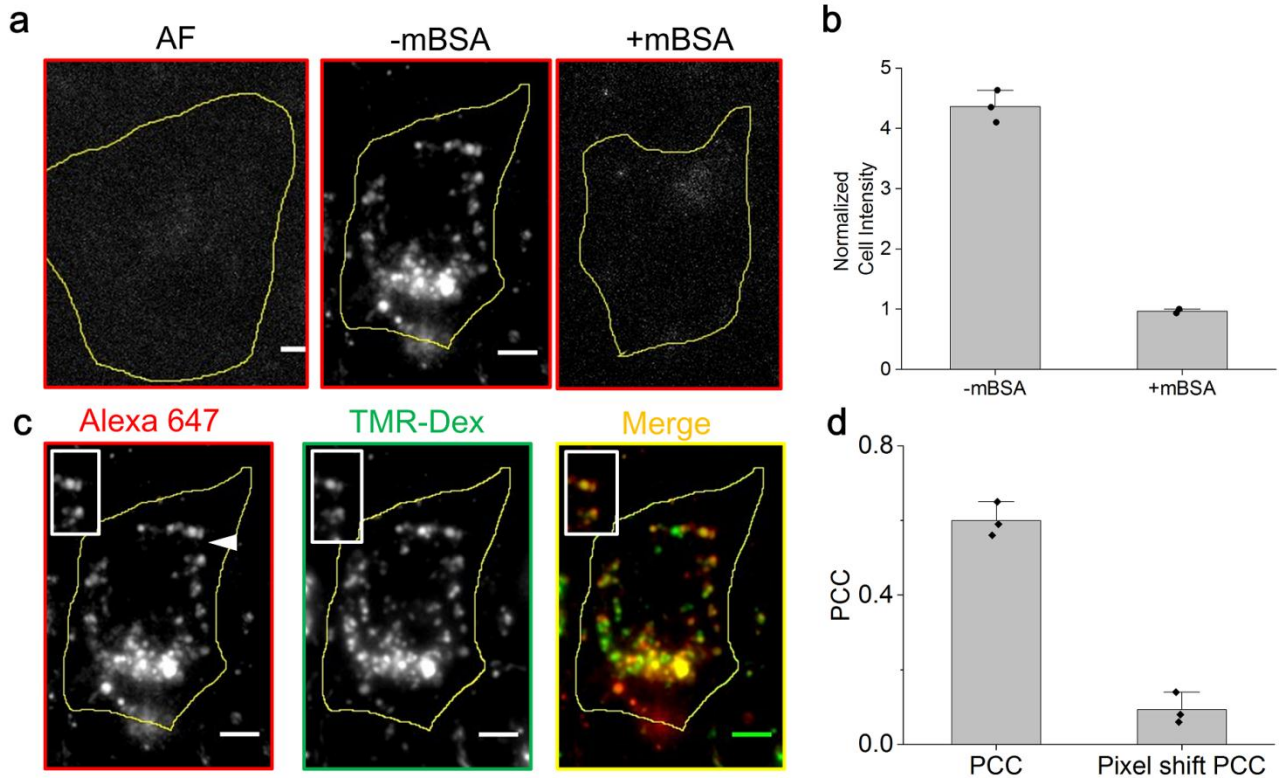

Supplementary Fig. 11 Labeling lysosome of T47D cells (**a**–**b**) *ChloropHore* internalization by T47D cells is competed out by excess maleylated BSA (mBSA, 10 μM), revealing uptake is by scavenger receptors. Cells are imaged in Alexa647 channel. (**c**) Representative images of lysosomes of T47D cells labelled with TMR dextran (TMR; G) by fluid phased endocytosis and by scavenger receptor mediated endocytosis of *ChloropHore* (Alexa647) and the corresponding Pearson's correlation coefficient for the colocalization is shown in (**d**). Experiments were performed in triplicate. Error bars indicate the mean of three independent experiments ± s.e.m. (n = 20 cells).

Before performing the 2-IM measurement in BHK-21, T47D and J774A.1 cells, we examined the trafficking time for sensors to reach lysosomes of these cells. Upon incubating *ChloropHore* (1 μM) with BHK-21 and T47D cells for 30 min (referred to as a 30 min "pulse") we found excellent uptake into punctate endosomes. The uptake was abolished in the presence of 10 equivalents of a competitor ligand for SRs e.g., maleylated BSA (mBSA)[9]. This revealed that in BHK-21 and T47D cells, *ChloropHore* is internalized *via* the SR-mediated endocytic pathway. To estimate the time required for lysosomal delivery of *ChloropHore*, we studied the time-dependent colocalization of *ChloropHore* with a lysosomal marker. Next, we pulsed *ChloropHore* for 30 min on BHK-21 and T47D cells whose lysosomes were pre-labeled with TMR-Dextran (TMR-Dex) as above, washed the cells and imaged them at various chase times. Colocalization of *ChloropHore* with TMR-Dex gradually increased reaching maximal co-localization at 90 and 60 min for BHK-21 and T47D cells respectively. Thus, *ChloropHore* is uptaken *via* scavenger receptor mediated endocytosis and robustly labels lysosomes in BHK-21 and T47D cells.

Two lysosomal populations observed in various cell types.

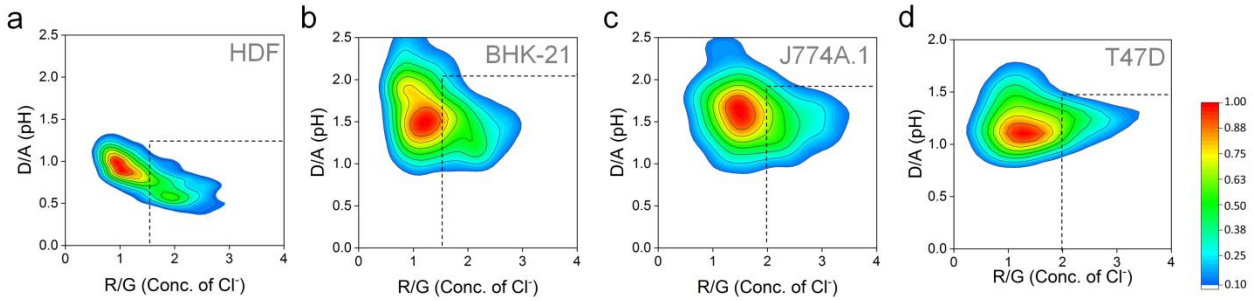

Supplementary Fig. 12 2-IM profiles of lysosomes in various cell types. 2-IM profiles of lysosomes in (**a**) human skin fibroblasts, (**b**) Baby hamster kidney fibroblasts, BHK-21, (**c**) murine macrophages J774A.1 and (d) T47D human breast cancer cell lines. Experiments were performed in duplicate (n = 55 cells, = 550 lysosomes)

To demonstrate the performance of *ChloropHore*$_{Ly}$ in other cell types, we performed the measurement and obtained the 2-IM profile of lysosomes in three other cell lines - (i) a macrophage cell line, such as J774A.1, as many lysosomal disorders manifest in macrophages (ii) BHK cells as these are rodent fibroblasts, compared to human fibroblasts in the main study and (iii) T-47D cells that are breast cancer cells of human origin, representing a different cell type from the main study. Please note that the threshold value for pH is changed, because lysosomes in all cell types do not show the same acidity levels. Nevertheless it is clear that these 2-IM profiles cannot be described as having only a monodisperse population of lysosomes. All 2-IM profiles display the common features that with high heterogeneity of lysosomes and a high chloride ion population.

Programming *ChloropHore* delivery to lysosome of fibroblasts

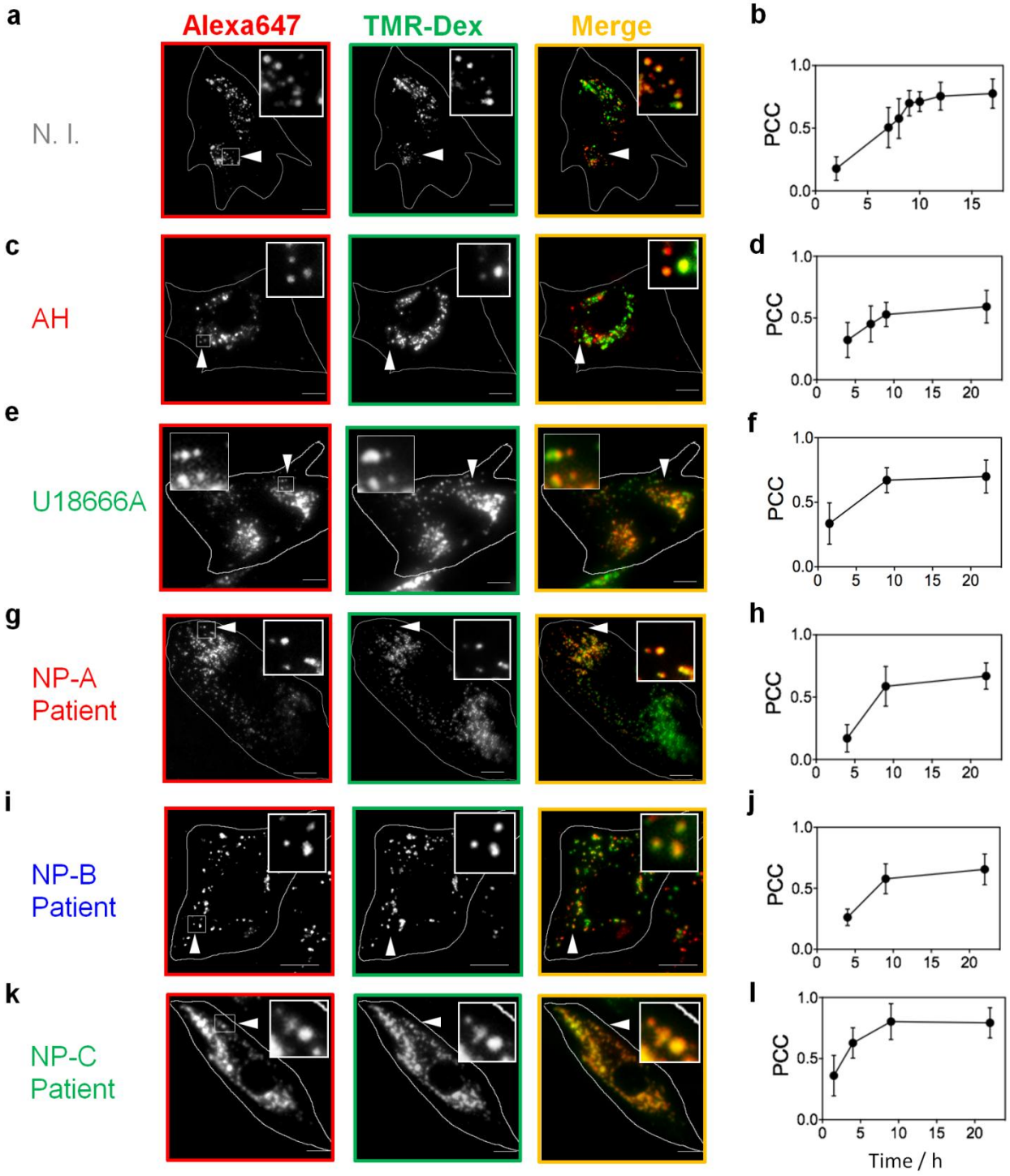

Supplementary Fig. 13 Lysosome labeling of endocytosed *ChloropHore* in fibroblasts. Representative images of lysosomes of (**a**) normal individual skin fibroblasts, (**c**) amitriptyline (AH)

induced NP-A/B model, (**e**) U18666A induced NP-C model, (**g**) NP-A patient derived skin fibroblasts, (**i**) NP-B patient derived skin fibroblasts and (**k**) NP-C patient derived skin fibroblasts labelled with TMR dextran (TMR-Dex) and *ChloropHore* (Alexa647) upon 1 h pulse and 9 h chase of *ChloropHore*. Pearson's correlation coefficient (PCC) for the colocalization between *ChloropHore* and lysosome marker – TMR Dextran in (**b**) normal individual skin fibroblasts, (**d**) amitriptyline (AH) induced NP-A/B model, (**f**) U18666A induced NP-C model, (**h**) NP-A patient derived skin fibroblasts, (**j**) NP-B patient derived skin fibroblasts and (**l**) NP-C patient derived skin fibroblasts at indicated chasing times. Scale bar = 10 mm and inset scale bar = 5 mm. Experiments were performed in triplicate. Error bars indicate the mean of three independent experiments ± s.e.m. (n = 25 cells).

We first established a protocol for efficient lysosome labeling by fluorescently labeled dextran. Human skin fibroblasts were transfected with LAMP1-RFP and pulsed and chased with FITC-Dex for different times, imaged and scored for colocalization (**Figure 2d–e**). We found that a 1 h pulse with *ChloropHore* followed by a 9 h chase is the minimum time to achieve quantitative lysosome labeling by FITC-Dex (**Figure 2f–g**). To investigate if acid sphingomyelinase and NPC1 deficiency lead to altered *ChloropHore* trafficking, we performed time-dependent co-localization experiments in amitriptyline (AH) induced NP-A/B model, U18666A induced NP-C model, NP-A, NP-B and NPC patient derived skin fibroblasts. A low Pearson's correlation coefficent (PCC) value was observed when $t < 5$ h and maximal colocalization is reached as early as $t = 9$ h. These results indicate that a 1 h pulse and 9 h chase of *ChloropHore* in ASM and NPC1 deficient cells reveals no trafficking delays.

We similarly evaluated skin fibroblasts derived from Niemann-Pick disease type A, type B patients and type C patient samples (**Supplementary Fig. S13**). Firstly, 0.25 mg/mL of lysosome marker TMR-Dex was pulsed for 1 h and chased for 16 h to label the lysosome. Next, 1 µM of *ChloropHore* was pulsed for 1 h and chased for various time points and co-localization between the lysosome marker and *ChloropHore* was assessed. We observed that *ChloropHore* is internalized into the cell and reaches lysosomes after a 9 h chase in all samples similar to wild type cells. Thus, no delays in probe trafficking to the lysosome was observed even in patient cells.

Reference

1. Modi, S., Nizak, C., Surana, S., Halder, S. & Krishnan, Y. Two DNA nanomachines map pH changes along intersecting endocytic pathways inside the same cell. *Nat Nanotechnol* **8,** 459–467 (2013).
2. Modi, S., Halder, S., Nizak, C. & Krishnan, Y. Recombinant antibody mediated delivery of organelle-specific DNA pH sensors along endocytic pathways. *Nanoscale* **6,** 1144–1152 (2014).
3. Gbadebo, A. M. & Nwufoh, C. O. Iodine concentrations in blood and urine samples of goitre and non-goitre patients in parts of Ogun State, Southwestern Nigeria. *Journal of geochemical exploration* **107,** 169–174 (2010).
4. Olszowy, H. A., Rossiter, J., Hegarty, J. & Geoghegan, P. Background levels of bromide in human blood. *J Anal Toxicol* **22,** 225–230 (1998).
5. Kapil, U. Health consequences of iodine deficiency. *Sultan Qaboos Univ Med J* **7,** 267–272 (2007).
6. Halder, S. & Krishnan, Y. Design of ultrasensitive DNA-based fluorescent pH sensitive nanodevices. *Nanoscale* **7,** 10008–10012 (2015).
7. Chakraborty, K., Leung, K. & Krishnan, Y. High lumenal chloride in the lysosome is critical for lysosome function. *elife* **6,** e28862 (2017).
8. Saha, S., Prakash, V., Halder, S., Chakraborty, K. & Krishnan, Y. A pH-independent DNA nanodevice for quantifying chloride transport in organelles of living cells. *Nat Nanotechnol* **10,** 645–651 (2015).
9. Gough, P. J. & Gordon, S. The role of scavenger receptors in the innate immune system. *Microbes Infect* **2,** 305–311 (2000).